Hybrid Quantum Model for Low-Energy Ion/Atom-Hydrogen Inelastic Collisions: Application to $Na^+ + H^-$ and Na+H

Yu Wang(王瑜)[1], Ting Gong(宫廷)[1], Chuanliang Li(李传亮)[1*], Kun Wang(王堃)[2*], Yukun Yang(杨玉坤)[3], Ling Liu(刘玲)[4*], Jinjun Liu(刘进军)[6], Béla Fiser[7], Svetlana A. Yakovleva[8*], Yong Wu(吴勇)[4,5], Jianguo Wang(王建国)[4], and Andrey K. Belyaev[8]

[1]*Shanxi Province Engineering Research Center of Precision Measurement and Online Detection Equipment, School of Applied Science, Taiyuan University of Science and Technology, Taiyuan 030024, China*
[2]*Institute of Environmental Science, Shanxi University, Taiyuan 030006, China*
[3]*School of Physics, Henan Normal University, Xinxiang 453000, China*
[4]*Key Laboratory of Computational Physics, Institute of Applied Physics and Computational Mathematics, Beijing 100088, China*
[5]*High Energy Density Physics, Center for Applied Physics and Technology, Peking University, Beijing 100084, China*
[6]*Department of Chemistry, University of Louisville, Louisville, Kentucky 40292, United States of America*
[7]*Institute of Chemistry, University of Miskolc, Miskolc-Egyetemváros 3515, Hungary*
[8]*Department of Theoretical Physics and Astronomy, Herzen University, St. Petersburg 191186, Russia*

(Received 4 December 2025; accepted manuscript online 6 January 2026)

A hybrid quantum model is introduced for low-energy ion/atom-hydrogen collisions. The model integrates *ab initio* calculations for low-lying states with asymptotic fitting for highly excited states, enabling fully quantum mechanical dynamics calculations that capture radial and rotational couplings across all internuclear distances, thereby addressing limitations of Landau–Zener models, which neglect short-range nonadiabatic interactions. Applied to the NaH system, the results for both mutual neutralization and excitation processes align well with fully quantum mechanical benchmarks for dominant channels. The analysis reveals the dominance of long-range ionic-covalent interactions for large cross sections and the significant influence of rotational coupling above 10 eV/u. Furthermore, discrepancies in weak excitation channels highlight the critical role of short-range non-adjacent couplings, which are often neglected in simplified models. This framework provides a robust tool for astrophysical non-local thermodynamic equilibrium modeling, thereby improving the accuracy of stellar abundance analyses.

DOI: 10.1088/0256-307X/43/2/020303 CSTR: 32039.14.0256-307X.43.2.020303

In modern astrophysics, determining stellar chemical compositions through high-resolution spectroscopy is a key research area.[1,2] Hydrogen, the universe's most abundant element and a key constituent of stellar cores, interstellar media, and planetary atmospheres, drives inelastic collisions with metal ions/atoms, significantly influencing non-local thermodynamic equilibrium (non-LTE) effects through deviations in radiative and collisional processes.[3,4] The era of multi-wavelength collaborative observations, with missions like RAVE,[5] Gaia-ESO,[6] Gaia,[7] XRISM,[8] Chandra *et al.*,[9] China's EP,[10] and HUBS,[11] has amassed vast spectral data, advancing studies of cosmic nucleosynthesis, stellar evolution, and baryon cycles. However, accurate non-LTE modeling relies on reliable rate coefficients for these collisions, where quantum effects in low-energy regimes, such as nonadiabatic transitions driven by ionic-covalent interactions, dominate the excitation and charge transfer processes.[4]

Early studies commonly used the Drawin formula to estimate inelastic collision data between ions/atoms and hydrogen atoms,[12–14] but its reliance on the classical Thomson model has been questioned for physical reliability.[3,15] To address this, Belyaev and Barklem *et al.* developed quantum approximate methods based on asymptotic approaches and the Landau–Zener (LZ) model, including multichannel LZ methods,[16–18] quantum branching probability current methods,[3,4] and simplified quantum methods,[19,20] etc. These methods are computationally efficient for multi-channel reactions and accurately describe optimal reaction windows between highly excited states, where long-range ionic-covalent interactions dominate, leading to avoided crossings that facilitate efficient nonadiabatic transitions. However, they simplify short- (even medium-) range nonadiabatic effects and neglect rotational coupling. Crucially, these simplified models typically restrict nonadiabatic transitions to adjacent adiabatic states, explicitly neglecting the couplings between non-adjacent channels. This simplification can cause deviations in cross sections for weak reaction channels up to 1–8 orders of magnitude, particularly at higher

*Corresponding authors. Email: clli@tyust.edu.cn; wang_kun@sxu.edu.cn; liu_ling@iapcm.ac.cn; cvetaja@gmail.com
© 2026 Chinese Physical Society and IOP Publishing Ltd. All rights, including for text and data mining, AI training, and similar technologies, are reserved.

energies ($\geq$100 eV/u) or in systems where indirect transitions via intermediate states are significant.[4,21] Incorporating complete coupling mechanisms, including short-range interactions, can significantly improve small-to-medium inelastic cross sections, especially at higher energies.[4]

Fully quantum mechanical (FQ) methods are optimal for low-energy heavy-particle (ion, atom, molecular) collisions, particularly in the energy regime below keV/u, where quantum effects, such as electronic correlations, become significant due to long interaction times. For instance, the fully quantum mechanical molecular orbital close-coupling (QMOCC) method[22–24] solves the Schrödinger equation incorporating radial and rotational couplings to yield precise scattering matrices and reaction cross sections. Unlike LZ models, which approximate nonadiabatic transitions at isolated avoided crossings, QMOCC captures couplings across the entire internuclear distance, enabling accurate treatment of multicenter quantum dynamics. The accuracy of this approach has been thoroughly validated in systems such as H^+-H,[25] He^+-He,[26] He-H,[27] $O^{6+/7+}$-H,[28,29] N^{4+}-He,[30] and N^{3+}-H,[31] etc. In principle, provided the molecular state basis is sufficiently complete, the QMOCC method can describe collision dynamics with high fidelity.[31] Nevertheless, its reliance on high-precision *ab initio* calculations renders the computation of numerous highly excited states impractical for complex systems, despite their essential role in non-LTE modeling.

Inelastic collision parameters for low-energy ion/atom-H systems are fundamental for astrophysical modeling, serving as key inputs for non-LTE analyses of stellar abundances and related phenomena. However, the reliability and completeness of existing collision data remain severely limited.[32] To enable accurate FQ dynamical simulations, a new large-scale method is urgently needed to enhance the accuracy and completeness of electronic structure calculations for ion/atom-H systems, particularly for highly excited states. Extending the asymptotic approach of Belyaev *et al.*[4] for long-range ionic-covalent interactions, a hybrid quantum model is proposed. It integrates high-precision *ab initio* methods for ground and low-lying excited states with asymptotic fitting for long-range Coulomb channels and high excitation states, with dynamical calculations performed using the QMOCC method. This framework combines the strengths of traditional LZ-based quantum approximate methods and FQ approaches: asymptotic methods accurately describe long-range core nonadiabatic regions but are less precise for short-range and low excitation state structures, while FQ methods, based on *ab initio* calculations, precisely capture these states and naturally incorporate rotational coupling effects absent in LZ-based methods. By extending electronic structures through asymptotic and *ab initio* methods, the model enables FQ dynamics, yielding theoretically superior accuracy. It leverages the insight that long-range nonadiabatic regions dominate large cross sections via optimal avoided crossings, while short-range regions provide quantum corrections in weaker channels and high-energy regimes.[4,33]

To evaluate the reliability and practicality of the proposed model, the NaH system is selected as the primary test case. This choice is motivated not only by its astrophysical significance and well-defined electronic structure but also by its status as a standard benchmark system in collision dynamics. The extensive availability of theoretical results derived from diverse methodologies—ranging from perturbative[34] and semiclassical[35] models to LZ approximations[1,36] and FQ treatments[37–39]—provides an exceptional opportunity for a rigorous comparative assessment. Capitalizing on this wealth of data, this work investigates both the Na^++H^- mutual neutralization reaction, which tests the model's description of strong long-range ionic-covalent interactions, and the excitation processes [Na(nl)+H $\rightarrow$ Na(n$'l'$)+H], which involve weaker reaction channels highly sensitive to the details of the full coupling matrix. Consequently, the present results are compared with comprehensive literature, enabling a multi-dimensional validation across different dynamical regimes.

The proposed model permits the use of any *ab initio* methods, including MRD-CI and Molpro, with the objective of accurately calculating the potential energy curves (PECs) and coupling terms for the ground and excited electronic states of the collision system. Specifically, the *ab initio* calculation must accurately capture the Coulomb channel formed by the main ionic states (e.g., Na^++H^-) in the short-to-medium internuclear distance region. This *ab initio*-derived structure is then utilized to apply asymptotic methods, as in Belyaev method,[4] to fit the long-range potential of the Coulomb channel, the potentials of other highly excited states, and the radial couplings between adjacent channels, thereby providing a comprehensive structural description. The present study is based on the NaH electronic structures calculated by Wang *et al.*[38] using the MRD-CI method, a variant of the configuration interaction (CI) method, which can effectively handle electron correlation while improving computational efficiency via multiple reference configurations and truncation techniques; details see Refs. [40,41]. It is worth noting that within the framework of the Born–Oppenheimer (BO) approximation, the radial coupling matrix elements generally do not vanish as the internuclear distance R tends to infinity. To eliminate this artifact, corrections such as electron translation factors (ETFs)[42,43] or reprojection methods[44] are typically required. In this work, the ETF correction is adopted, following the procedure described by Wang *et al.*[38] These structures will be subjected to asymptotic fitting for model verification, thus avoiding redundant *ab initio* calculations for this specific system.

Subsequently, asymptotic methods are employed to fit the long-range potential energies and coupling terms for the high excitation states, following Belyaev method.[4] The central objective of this procedure is to fit the structure of the core ionic channel (i.e., the Coulomb channel) derived from the *ab initio* data, thereby accurately describing and extrapolating the positions and strengths of the

nonadiabatic interactions between this ionic channel and all other highly excited states. The potential energy (or diagonal elements of the Hamiltonian matrix), $H_{jj}(R)$, are formulated by combining analytical long-range and short-range components,[4]

$$H_{jj}(R) = A_j \mathrm{e}^{-\gamma_j R} + \frac{Z_\mathrm{A}}{R}\mathrm{e}^{-\tau R} + E_j^\infty - \frac{1-\mathrm{e}^{-\tau R^2}}{R}, \quad (1)$$

where the first term represents the exponential short-range exchange potential, the parameters A_j and γ_j are determined by fitting the *ab initio* potential energy data. The second term represents a short-range screened nuclear repulsion component, common to both ionic and covalent states, where Z_A is the nuclear charge of atom A. The third term, E_j^∞, denotes the asymptotic energy of the two particles as the internuclear distance $R \to \infty$. The final term is an additional long-range correction. For the ionic states ($\mathrm{A}^+ + \mathrm{H}^-$), the long-range potential is predominantly Coulombic; the parameter τ acts as a screening/damping factor and is obtained by fitting the Coulomb potential to the *ab initio* data. For the covalent states (A^*+H), the last term can typically be neglected, as dispersion forces are weaker.

The non-diagonal Hamiltonian elements (H_{ij}) between ionic and covalent states at the avoided crossing points are determined using the semi-empirical Olson–Smith–Bauer formula,[45] which is derived from the principles of single-electron exchange,

$$H_{\mathrm{ion},j}(R_\mathrm{c}) = \frac{\sqrt{-E_j}+\sqrt{-E_{\mathrm{H}^-}}}{\sqrt{2}}\sqrt{E_j E_{\mathrm{H}^-}}R_\mathrm{c} \times \mathrm{e}^{-0.86R_\mathrm{c}\frac{\sqrt{-E_j}+\sqrt{-E_{\mathrm{H}^-}}}{\sqrt{2}}}, \quad (2)$$

where R_c is the internuclear distance of the avoided crossing; E_j and E_{H^-} represent the ionization potential of $\mathrm{A}^*(j)$ and H^-, respectively. This formula is validated by Olson *et al.*[45] through a least-squares fit to H_{ij} and crossing points in 99 diverse systems, with 83% of data points within three standard deviations and a 95% confidence level. In the proposed model, non-diagonal matrix elements between covalent states are neglected, and adiabatic PECs are obtained by diagonalizing the resulting Hamiltonian matrix.

In the adiabatic representation, the radial coupling matrix elements at avoided crossings exhibit a Lorentzian form,[33] expressed as

$$\left\langle i\middle|\frac{\partial}{\partial R}\middle|f\right\rangle = \frac{\eta}{(R-R_\mathrm{c})^2+4\eta^2}, \quad (3)$$

where $\eta = H_{if}/|H'_{ii}-H'_{ff}|$ relates to the diabatic Hamiltonian, H_{if} is the non-diagonal Hamiltonian, while H'_{ii} and H'_{ff} are the first derivatives of the diagonal Hamiltonians with respect to R. This form arises from the perturbation theory approximation of nonadiabatic transitions, capturing the resonant energy transfer near R_c, where the integral over R approaches $\pi/2$.[33]

Although the presented formula involves multiple parameters, the primary goal of this method is to asymptotically estimate the electronic structures of highly excited and ionic states in the long-range nonadiabatic region, where *ab initio* calculations are challenging. In this long-range domain, the matrix elements are predominantly determined by the single parameter τ, which effectively describes the long-range PECs of the highly excited states by modulating the Coulomb tail. While the short-range potential comprises several parameters, the actual calculations for the ground and lower excited states utilize the accurate *ab initio* structures. Moreover, the impact of the short-range potential for high excited states in low-energy collisions is limited, as these regions contribute mainly through short-range partial waves, with negligible effects on large cross sections dominated by long-range interactions.

Based on the complete *ab initio* electronic structure data provided by Wang *et al.*,[38] the NaH system was fitted using the asymptotic method to obtain all parameters: nuclear charge of atom A (i.e., Na) $Z_\mathrm{A} = 11$, $\tau = 0.973$; ionic state short-range potential parameters $A_i = 8.99$, $\gamma_i = 1.60$; covalent state parameters $A_\mathrm{c} = 0.405$, $\gamma_\mathrm{c} = 1.044$. This yields the adiabatic PECs and radial coupling matrix elements (CMEs) for NaH, compared with Wang *et al.*'s MRD-CI results[38] (see Fig. 1). Figure 1(a) illustrates the pronounced long-range Coulomb effect from the ionic state Na^++H^- ($R > 10$ a.u.) and a series of avoided crossings in the adiabatic representation, where energy splittings dictate transition probabilities, as smaller splittings enhance nonadiabatic interaction due to stronger overlap of wavefunctions. Figures 1(b)–1(g) display radial CMEs from MRD-CI (solid lines) and the asymptotic method (Lorentzian fitting, dashed lines).

Overall, both methods agree well on the long-range PEC trends and the positions of avoided crossings. The radial CME strengths exhibit an inverse proportionality to the energy splittings at the crossings. Specifically, larger MRD-CI splittings at 6.95 a.u. ($1^1\Sigma^+$–$2^1\Sigma^+$) and 12.60 a.u. ($2^1\Sigma^+$–$3^1\Sigma^+$) yield slightly lower CME peaks in Figs. 1(b) and 1(c); consistent splittings at 21.42 a.u. ($3^1\Sigma^+$–$4^1\Sigma^+$) match CME peaks in Fig. 1(d); while smaller MRD-CI splittings at 34.40 a.u. ($4^1\Sigma^+$–$5^1\Sigma^+$) and 38.23 a.u. ($5^1\Sigma^+$–$6^1\Sigma^+$) result in much stronger CME peaks in Figs. 1(e) and 1(f) relative to fits. Figure 1(g) zooms in on the $4^1\Sigma^+$–$5^1\Sigma^+$ CME at 34.40 a.u.: MRD-CI exhibits a narrow, tall interaction region, versus the broad, low asymptotic fit; both integrate to $\approx\pi/2$ over R, implying comparable transition probabilities.[33] Notably, the MRD-CI calculations are limited in scope and do not include the radial CMEs between $6^1\Sigma^+$ and $7^1\Sigma^+$. Nevertheless, the asymptotic method yields results [as indicated by the blue dashed line in Fig. 1(f)] that reveal a pronounced coupling effect at 71.20 a.u., underscoring the model's ability to extrapolate beyond *ab initio* limits. Furthermore, the asymptotic fits indicate avoided crossing positions between higher-lying states—$7^1\Sigma^+$–$8^1\Sigma^+$ at approximately 187.89 a.u., $8^1\Sigma^+$–$9^1\Sigma^+$ at 194.23 a.u., and $9^1\Sigma^+$–$10^1\Sigma^+$ at 324.42 a.u.—characterized by extremely narrow interaction ranges ($<10^{-5}$ a.u.) yet exceptionally strong coupling strengths ($>10^6$ a.u.). In the present calculations,

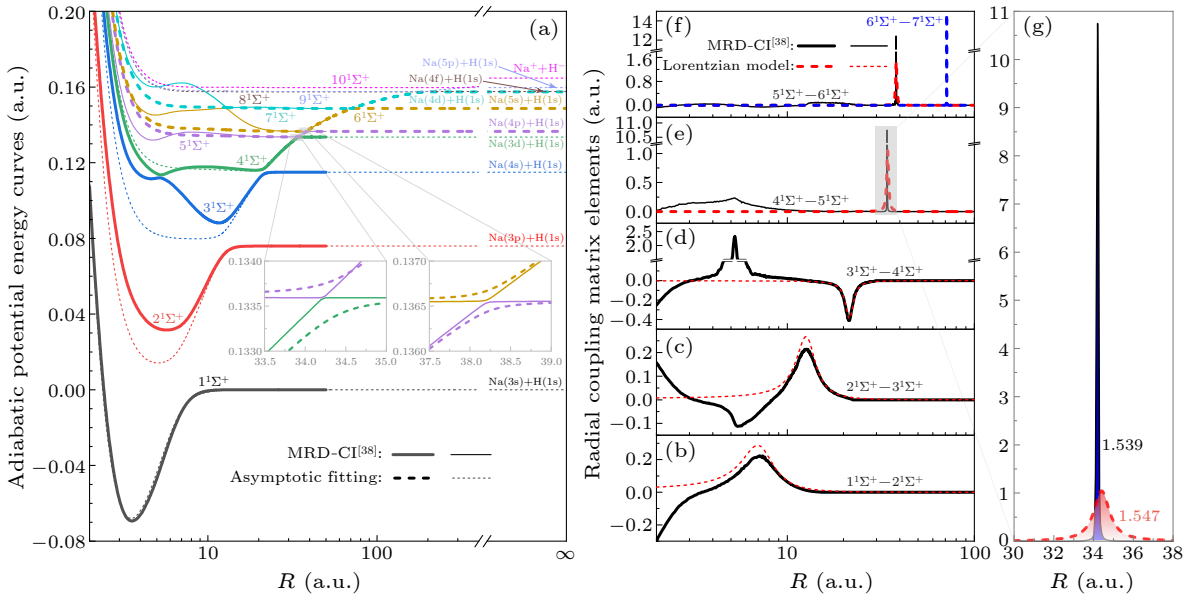

Fig. 1. Comparison of the asymptotic fitting results of the adiabatic PECs and radial CMEs of the NaH molecule with the MRD-CI results of Wang *et al.*[38] Panel (a): Low-lying PECs (MRD-CI solid lines, asymptotic fit dashed lines). Panels (b)–(g): Radial CMEs between specific $^1\Sigma^+$ states (MRD-CI solid lines, Lorentzian fit dashed lines). Bold lines highlight electronic potentials and couplings that will be used as the input of QMOCC.

the corresponding channels, Na(4d/4f/5p)+H, are omitted, as they contribute negligibly small cross sections[4] while necessitating significantly finer integration steps ($<10^{-6}$ a.u.) and extended integration ranges, thereby increasing computational cost by several orders of magnitude in FQ dynamics calculations.

Dynamical calculations are performed using the QMOCC method. Unlike dynamics based on the LZ model, which accounts only for nonadiabatic interactions (equivalent to radial couplings) between covalent and ionic states at long-range avoided crossings, QMOCC incorporates radial couplings between states of identical symmetry ($\Delta L = 0$) and rotational couplings between states of different symmetry ($\Delta L = 1$), across the entire internuclear distance R. This comprehensive treatment captures more quantum coherence effects.

The QMOCC method precisely describes atom–molecule collision dynamics, utilizing electronic wave functions for electron motion and treating nuclear motion in a FQ manner.[22,23] Starting from the Schrödinger equation, within the framework of the BO approximation and the perturbative stationary-state approximation, the radial channel function column vector $\boldsymbol{f}^J(R)$ for nuclear motion satisfies the following coupled differential equations in the adiabatic representation:

$$\left[\frac{\mathrm{d}^2}{\mathrm{d}R^2} + \frac{\lambda^2 - J(J+1)}{R^2} + 2\mu E\right]\boldsymbol{f}^J(R) = \left[2\mu \boldsymbol{V}^{\mathrm{P}}(R) + \boldsymbol{V}^{\mathrm{R}}(R) + \boldsymbol{V}^{\mathrm{C}}(R)\right]\boldsymbol{f}^J(R), \tag{4}$$

where μ is the reduced mass, E is the collision energy, $\boldsymbol{V}^{\mathrm{P}}(R)$ is the matrix representing the adiabatic potential energy, and $\boldsymbol{V}^{\mathrm{R}}(R)$ and $\boldsymbol{V}^{\mathrm{C}}(R)$ are the matrices representing the adiabatic radial and rotational couplings, respectively.

To remove the singularities in $\boldsymbol{V}^{\mathrm{R}}(R)$ and enhance numerical stability, the electronic structure must be converted from the adiabatic representation to the diabatic representation via a unitary transformation. The unitary matrix $\boldsymbol{C}(R)$ is introduced to transform the radial functions: $\boldsymbol{f}^J(R) = \boldsymbol{C}(R)\boldsymbol{g}^J(R)$. This transformation preserves the form of the coupled equations, but all electronic structure matrices $\boldsymbol{V}(R)$ are converted to their diabatic forms ${}^{\mathrm{d}}\boldsymbol{V}(R)$:

$${}^{\mathrm{d}}\boldsymbol{V}(R) = \boldsymbol{C}^{\dagger}(R)\boldsymbol{V}(R)\boldsymbol{C}(R). \tag{5}$$

Crucially, to ensure the validity of the transformation and eliminate the singularities in $\boldsymbol{V}^{\mathrm{R}}(R)$, the transformation requires that the matrix $\boldsymbol{A}$ (which arises from the radial coupling operator $\partial/\partial R$) satisfies: $\boldsymbol{A}\boldsymbol{C}(R) + \frac{\partial}{\partial R}\boldsymbol{C}(R) = \boldsymbol{0}$, with the condition that $\boldsymbol{C}(R) \to \boldsymbol{I}$ (the identity matrix) in the asymptotic region $R \to \infty$.

The resulting diabatic coupled equations are solved using the Johnson logarithmic derivative method.[46] In the asymptotic region $R \to \infty$, the channel functions $\boldsymbol{g}^J(R)$ are matched to the plane-wave boundary conditions:

$$g_i^J(R) \xrightarrow[R\to\infty]{} \frac{1}{\sqrt{k_j}}\Big[\delta_{ij} j_J(k_i R) + \boldsymbol{K}_{ij}^J \eta_J(k_j R)\Big], \tag{6}$$

where j_J and η_J are the regular and irregular Bessel–Riccati function solutions (or the corresponding Coulomb function solutions for Coulomb channels[47]). The reaction matrix $\boldsymbol{K}$ is thus computed, allowing the determination of the collision scattering $\boldsymbol{S}$ matrix,

$$\boldsymbol{S}_{ij}^J = \frac{\boldsymbol{I} + \mathrm{i}\boldsymbol{K}_{ij}^J}{\boldsymbol{I} - \mathrm{i}\boldsymbol{K}_{ij}^J}. \tag{7}$$

The total collision cross section σ_{ij} from channel i to

j is then given by

$$\sigma_{ij} = \frac{\pi\hbar^2 p_i^{\rm stat}}{k_i^2} \sum_J (2J+1)|\boldsymbol{S}_{ij}^J|^2, \tag{8}$$

where $p_i^{\rm stat}$ is the statistical probability for the initial channel i, and k_i is the initial center-of-mass momentum.

For application to the NaH system, we select MRD-CI-derived PECs and radial CMEs for the $1^1\Sigma^+$ to $4^1\Sigma^+$ states (bold solid lines in Fig. 1), along with asymptotic PECs and radial CMEs for the $5^1\Sigma^+$ to $7^1\Sigma^+$ states (bold dashed lines in Fig. 1), as QMOCC inputs. It should be noted that, for diabatization procedure, the ion-channel PECs are directly spliced to ensure convergence to the correct dissociation limit in the long-range region ($R \geq 178$ a.u.). The limitations of the proposed model lie in its inability to estimate rotational coupling effects. In the NaH system, to maximally assess the reliability of the current model relative to the LZ method, we adopt inputs consistent with those used in LZ approaches by omitting the Π-state PECs and rotational CMEs between Π and Σ states. The results are then compared with QMOCC calculations by Wang *et al.*,[38] which incorporate complete MRD-CI structural data encompassing all radial and rotational couplings, to validate the reliability of our model.

Figure 2 presents the total cross sections for the Na^++H^- mutual neutralization reaction over 0.001–1000 eV/u, computed by using the proposed model, incorporating $7^1\Sigma^+$ states. Overall, the results align in trend and magnitude with prior theories.[1,34–38] Below 1 eV/u, the cross section exhibits an E^{-1} dependence, a hallmark of s-wave dominated scattering in low-energy quantum regimes where extended interaction times enhance nonadiabatic probabilities. Above this threshold, the cross section decreases gradually, with a slowing decay rate, consistent with patterns observed in analogous systems like Li^+, Cs^+, and H^- mutual neutralizations.[1,36,48] Discrepancies among methods emerge primarily in the energy regime above 1 eV/u: the LZ models exhibit a sharp decline in cross sections with increasing energy, particularly the LCAO-based results of Barklem *et al.*[1] (incorporating $9^1\Sigma^+$ states), whereas the Landau–Herring-based model by Janev *et al.*[36] (with $6^1\Sigma^+$ states) shows a delayed acceleration in decay until around 100 eV/u, highlighting the limitations of LZ approximations in high-energy regimes where multi-channel effects and velocity-dependent couplings are inadequately captured. FQ approaches[37,38] yield broadly consistent trends by more accurately resolving nonadiabatic dynamics; however, QMOCC results based on complete MRD-CI data of Wang *et al.*,[38] incorporating $7^1\Sigma^+$ states and $3^1\Pi$ states, produce substantially larger cross sections after 20 eV/u, attributable to the present work's omission of rotational couplings and short-range avoided crossings (e.g., the strong nonadiabatic interaction between the $6^1\Sigma^+$ and $7^1\Sigma^+$ states at 12.90 a.u.), which become increasingly relevant as energy rises and higher partial waves contribute. In contrast, FQ results of Dickinson *et al.*,[37] which consider $10^1\Sigma^+$ states without Π states, yield slightly lower values

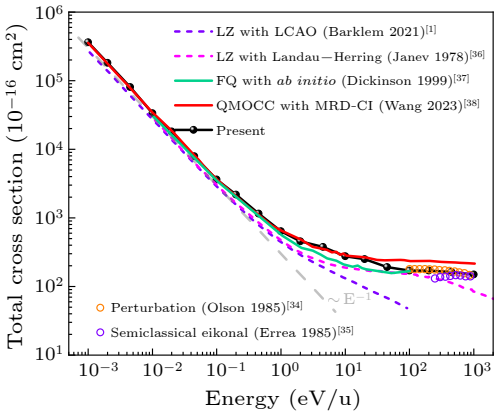

Fig. 2. Total cross sections for the mutual neutralization reaction $Na^+ + H^- \rightarrow Na(nl)+H$. Present results (black solid line with filled circles) compared with QMOCC by Wang *et al.*[38] (red solid line), FQ result by Dickinson *et al.*[37] (green solid line), LZ models by Janev *et al.*[36] (pink dashed line) and Barklem *et al.*[1] (purple dashed line), perturbation theory by Olson *et al.*[34] (orange circles), and semiclassical method by Errea *et al.*[35] (purple circles).

in the 1–100 eV/u range compared to the present results, likely stemming from methodological differences in handling details such as long-range fitting parameters and maximum internuclear distance integration limits. The semiclassical calculations by Errea *et al.*,[35] limited to five $^1\Sigma^+$ states, result in a slightly poorer agreement above 100 eV/u, while the perturbation method of Olson *et al.*,[34] incorporating five $^1\Sigma^+$ states and two $^1\Pi$ states, achieves a significantly better match in this regime despite both excluding higher-lying excited states [e.g., Na(4p) and Na(5s)].

Figures 3(a)–3(f) illustrate the state-selected cross sections for the mutual neutralization reaction $Na^+ + H^- \rightarrow Na(nl)+H$ across the energy range from 0.001 to 1000 eV/u. Overall, the present results exhibit quantitative agreement in both trend and magnitude with the FQ calculations by Dickinson *et al.*[37] and Wang *et al.*,[38] with deviations generally confined to within one order of magnitude. The cross section for electron transfer to the Na(4s) state [Fig. 3(c)] yields the largest values, with results from all methods nearly overlapping, underscoring the robustness of both quantum and approximate approaches for dominant channels. The cross sections for transfers to the Na(3d) [Fig. 3(d)] and Na(4p) [Fig. 3(e)] states are the next largest, where deviations—including those from LZ models—remain within one order of magnitude, highlighting the reliability of LZ methods for principal reaction pathways at low-energy collisions. For the Na(3d) channel [Fig. 3(d)], the present results are lower than Wang *et al.*'s[38] above 10 eV/u, primarily due to the omission of rotational couplings, which enhance contributions from higher angular momentum states at elevated energies. For the Na(4p) channel [Fig. 3(e)], the present results are slightly higher in the low-energy region and lower at higher energies—attributable to the neglect of the short-range strong nonadiabatic interaction between the $6^1\Sigma^+$ and $7^1\Sigma^+$ states at 12.90 a.u. (causing the higher values

at low energies) and of rotational couplings (leading to the lower values at high energies). Notably, Dickinson *et al.*'s results,[37] which incorporate more complete *ab initio* data for $^1\Sigma^+$ states than those of Wang *et al.*[38] but without rotational coupling effects, align well with Wang *et al.*'s results[38] below 5 eV/u yet diverge toward lower values above this threshold.

For the Na(5s) channel [Fig. 3(f)], the present model aligns closely with Dickinson *et al.*,[37] but deviates more from Wang *et al.*,[38] potentially linked to the long-range strong nonadiabatic interaction between the $6^1\Sigma^+$ and $7^1\Sigma^+$ states at 71.20 a.u., which MRD-CI calculations do not include and thus omit from Wang *et al.*'s QMOCC dynamics.[38] In contrast, the present asymptotic fitting incorporates this coupling, yielding results more consistent with Dickinson *et al.*'s approach.[37] This demonstrates the model's advantage in long-range fitting, enabling comparable accuracy with substantial computational savings. The cross sections for transfers to the Na(3s) [Fig. 3(a)] and Na(3p) [Fig. 3(b)] states represent weaker channels, where both the present model and LZ approaches show larger deviations relative to FQ benchmarks, with errors increasing for progressively weaker pathways. However, while LZ models[36] can overestimate by up to three orders of magnitude, the present results maintain consistent trends across the entire energy range, with deviations stabilized within one order of magnitude. This strong agreement robustly validates the high accuracy and reliability of the proposed model in capturing long-range Coulomb asymptotics and nonadiabatic couplings for low-lying excited states. The fundamental source of LZ errors lies in its inadequate description of the electronic structure and associated nonadiabatic interactions for ground and lower excited states.

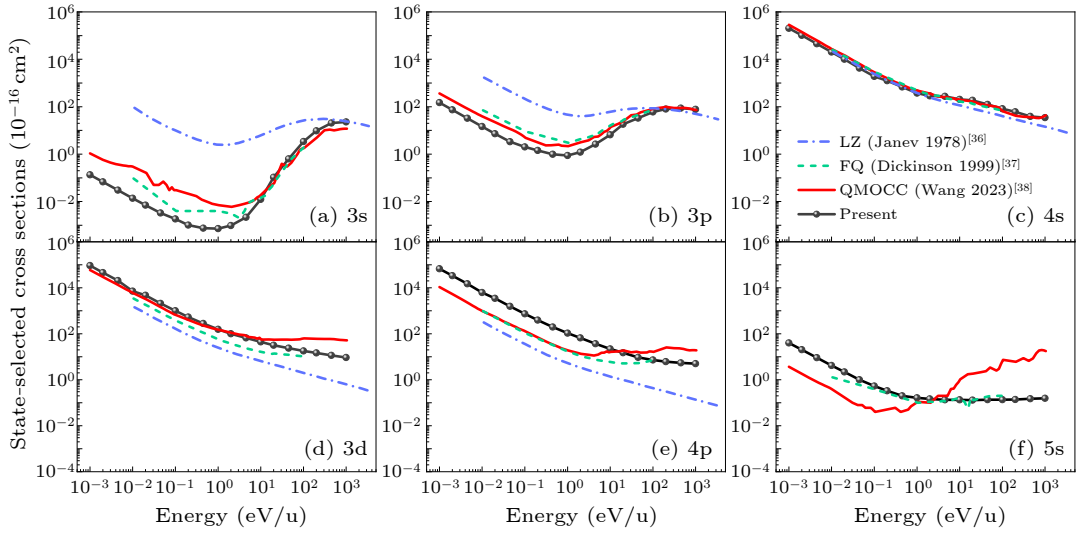

Fig. 3. State-selected cross sections for the mutual neutralization reaction $Na^+ + H^- \rightarrow Na(nl) + H$. Present results (black solid line with filled circles) compared with QMOCC by Wang *et al.*[38] (red solid line), FQ result by Dickinson *et al.*[37] (green dashed line), and LZ models by Janev *et al.*[36] (blue dash-dotted line).

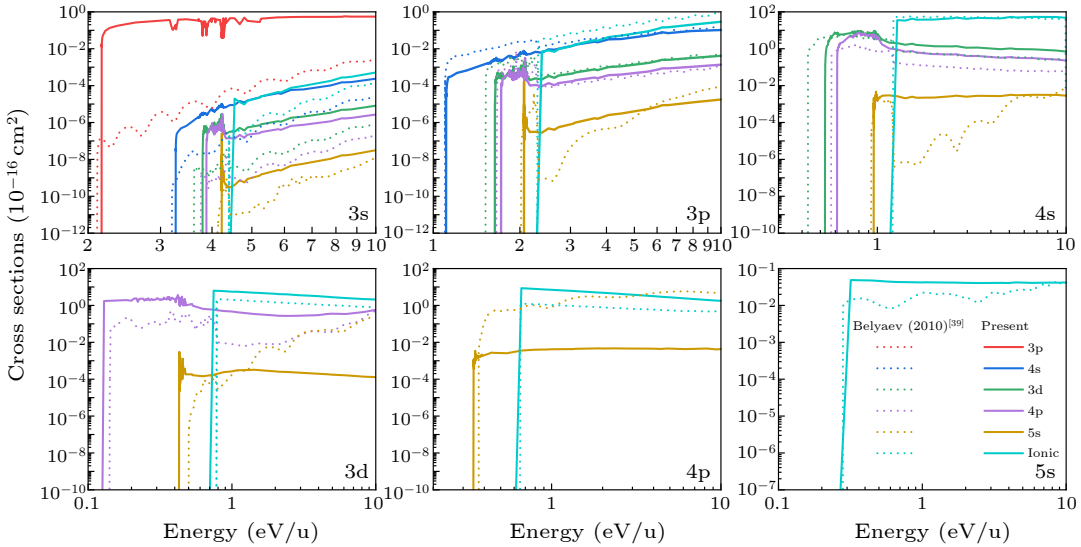

Fig. 4. State-selected cross sections for the Na(nl)+H collision system, specifically showing the excitation to various final Na(nl) (nl = 3s, 3p, 4s, 3d, 4p, and 5s) states and charge transfer to the ionic channel ($Na^+ + H^-$). Present results (solid line) are compared with the calculation by Belyaev *et al.*[39] (dashed line).

To further rigorously test the model's capability in describing processes dominated by different coupling mechanisms, the cross sections for the excitation processes were calculated. Figure 4 presents the state-selected electron excitation cross sections for the Na+H collision system, spanning the energy range of 0.1 eV/u to 10 eV/u for selected final states (nl = 3s, 3p, 4s, 3d, 4p, 5s), alongside the cross section for the ionic channel. The present calculations, which cover 21 distinct reaction processes, are compared against the prior full quantum-mechanical theoretical results from Belyaev *et al.*,[39] which utilized a 10-adiabatic $^1\Sigma^+$ state molecular basis. Overall, the results of the present method demonstrate good consistency with the existing literature regarding the energy dependency of the vast majority of excitation channels, with the magnitude discrepancies generally stabilizing within 1 to 2 orders of magnitude. The consistency is particularly high at the high-energy end, where most channels show near-perfect agreement. However, the neglect of radial coupling effects between non-adjacent channels leads to very significant discrepancies in the detailed structure and absolute magnitude for certain weak reaction channels. For instance, the cross section for the 3s → 3p excitation process is overestimated by up to seven orders of magnitude at low collision energies. This pronounced overestimation stems from the lack of non-adjacent coupling, which artificially enhances the direct excitation probability from the 3s state to the 3p state; including the full coupling would instead distribute the probability to other channels, thereby lowering the 3s → 3p cross section. Furthermore, the results for excitation to the 5s state exhibit substantial errors, notably the 4p → 5s process, which is underestimated by nearly four orders of magnitude at low energies. This underestimation is potentially related to the use of a fitted Lorentzian-type function for the radial coupling, which may overlook some weak coupling effects at intermediate and small internuclear distances, resulting in a systematic underestimation across the entire energy range.

This work introduces a hybrid quantum framework that extends Belyaev's asymptotic methods[4,33] by integrating *ab initio* calculations for low-lying states with semi-empirical fitting for higher excitations, enabling FQ dynamics via QMOCC. Applying this model to the benchmark NaH system, we performed a comprehensive validation covering both Na^++H^- mutual neutralization and Na+H excitation processes. The results for mutual neutralization and dominant excitation channels quantitatively align with high-precision quantum benchmarks, confirming that accurate asymptotic fitting of long-range ionic-covalent interactions is sufficient to capture the physics of large cross sections. However, a critical physical insight emerges from the analysis of weak excitation channels. Specifically, the comparison for the Na(3s) → Na(3p) transition reveals that neglecting radial couplings between non-adjacent channels leads to significant discrepancies—up to seven orders of magnitude—in the low-energy regime. This finding underscores that while simplified coupling schemes are robust for dominant pathways, the subtle quantum interference effects governing weak transitions are heavily modulated by short-range, non-adjacent interactions. Additionally, the results confirm the pronounced role of rotational couplings involving Π states in the high-energy regime (>10 eV/u), where their omission results in systematic deviations. In summary, while the omission of non-adjacent couplings limits accuracy for specific weak transitions at low energies, the proposed hybrid model successfully balances computational efficiency with dynamical rigor for astrophysically relevant processes. It provides a powerful tool for generating reliable large-scale collision data for complex systems (e.g., O^{n+}-H/He), thereby improving the precision of non-LTE stellar abundance analyses.

Acknowledgements. This work was supported by the National Natural Science Foundation of China (Grant Nos. 12274040, 12504297, 12204288, 12304279, and 62475182), the National Key R&D Program of China (Grant No. 2022YFA1602504), the Shanxi Province Scientific Research Initial Funding (Grant No. 20252011), the Taiyuan University of Science and Technology Scientific Research Initial Funding (Grant No. 20242149), the Special Fund for Science and Technology Innovation Teams of Shanxi Province (Grant No. 202304051001034), the Key Research and Development Program of Shanxi Province (Grant Nos. 202402150301012 and 202402130501005), and the Central Guidance on Local Science and Technology Development Fund of Shanxi Province (YDZJSX2025C026). The work of SAY and AKB was supported by an internal grant of Herzen University (Project No. 46-VG).

References

[1] Barklem P S, Amarsi A M, Grumer J, Eklund G, Rosén S, Ji M C, Cederquist H, Zettergren H, and Schmidt H T 2021 *Astrophys. J.* **908** 245
[2] Asplund M 2005 *Annu. Rev. Astron. Astrophys.* **43** 481
[3] Belyaev A K and Voronov Y V 2018 *Astrophys. J.* **868** 86
[4] Belyaev A K 2013 *Phys. Rev. A* **88** 052704
[5] Kunder A, Kordopatis G, Steinmetz M *et al.* 2017 *Astron. J* **153** 75
[6] Sacco G G, Morbidelli L, Franciosini E *et al.* 2014 *Astron. Astrophys.* **565** A113
[7] Titarenko A, Recio-Blanco A, de Laverny P, Hayden M, and Guiglion G 2019 *Astron. Astrophys.* **622** A59
[8] Tashiro M S 2022 *Int. J. Mod. Phys. D* **31** 2230001
[9] Weisskopf M C, Tananbaum H D, Van Speybroeck L P, and O'Dell S L 2000 *Proc. SPIE* **401** 2
[10] Yuan W M, Zhang C, Chen Y *et al.* 2018 *Sci. Sin. Phys. Mech. Astron.* **48** 039502
[11] Cui W, Chen L B, Gao B *et al.* 2020 *J. Low Temp. Phys.* **199** 502
[12] Drawin H W 1968 *Z. Phys. A* **211** 404
[13] Drawin H W 1969 *Z. Phys. A* **225** 483
[14] Lambert D L 1993 *Phys. Scr.* **T47** 186
[15] Barklem P S, Belyaev A K, Guitou M, Feautrier N, Gadéa F X, and Spielfiedel A 2011 *Astron. Astrophys.* **530** A94
[16] Belyaev A K 1993 *Phys. Rev. A* **48** 4299
[17] Yakovleva S A, Voronov Y V, and Belyaev A K 2016 *Astron. Astrophys.* **593** A27

[18] Barklem P S 2016 *Phys. Rev. A* **93** 042705
[19] Belyaev A K and Yakovleva S A 2017 *Astron. Astrophys.* **606** A147
[20] Belyaev A and Yakovleva S 2017 *Astron. Astrophys.* **608** A33
[21] Liu X J, Wang J G, Qu Y Z, and Buenker R J 2011 *Phys. Rev. A* **84** 042706
[22] Zygelman B, Cooper D L, Ford M J, Dalgarno A, Gerratt J, and Raimondi M 1992 *Phys. Rev. A* **46** 3846
[23] Bransden B H and McDowell M R C 1992 *Charge Exchange and The Theory of Ion-Atom Collisions* (Oxford: Clarendon Press)
[24] Nolte J L, Stancil P C, Liebermann H P, Buenker R J, Hui Y, and Schultz D R 2012 *J. Phys. B: At. Mol. Opt. Phys.* **45** 245202
[25] Wang Y, Wang K, Liu L, Wu Y, Wang F, and Wang J G 2024 *Astrophys. J. Suppl. Ser.* **272** 39
[26] Wang Y, Wang F, Lin X H, Liu L, Wu Y, and Wang J G 2023 *Astron. Astrophys.* **674** A201
[27] Wang K, Dong C, Qu Y Z, Liu L, Wu Y, Hong X H, and Buenker R J 2022 *Chin. Phys. B* **31** 123401
[28] Lin X H, Wu Y, Wang J G, Shao B, and Janev R K 2019 *Astron. Astrophys.* **625** A123
[29] Lin X H, Wang K, Wang Y, Liu L, Wu Y, Lin M J, Li R, and Wang J G 2023 *Astron. Astrophys.* **679** A67
[30] Wang K, Wang X X, Qu Y Z, Liu C H, Liu L, Wu Y, and Buenker R J 2020 *Chin. Phys. Lett.* **37** 023401
[31] Lin X H, Lin M J, Wang K, Wu Y, Ren Y, Wang Y, and Li J W 2025 *Acta Phys. Sin.* **74** 152501 (in Chinese)
[32] Lyons D, Cumbee R S, and Stancil P C 2017 *Astrophys. J. Suppl. Ser.* **232** 27
[33] Belyaev A K 2007 *Eur. Phys. J. D* **44** 497
[34] Olson R E and Kimura M 1985 *Phys. Rev. A* **32** 3092
[35] Errea L F, Méndez L, Mó O, and Riera A 1986 *J. Chem. Phys.* **84** 147
[36] Janev R K and Radulović Z M 1978 *Phys. Rev. A* **17** 889
[37] Dickinson A S, Poteau R, and Gadéa F X 1999 *J. Phys. B: At. Mol. Opt. Phys.* **32** 5451
[38] Wang K, Dong C, Qu Y Z, Wu Y, Lin X H, and Buenker R J 2023 *Chin. Phys. B* **32** 083103
[39] Belyaev A K, Barklem P S, Dickinson A S, and Gadéa F X 2010 *Phys. Rev. A* **81** 032706
[40] Buenker R J and Phillips R A 1985 *J. Mol. Struct.: THEOCHEM* **123** 291
[41] Krebs S and Buenker R J 1995 *J. Chem. Phys.* **103** 5613
[42] Gargaud M, McCarroll R, and Valiron P 1987 *J. Phys. B: At. Mol. Phys.* **20** 1555
[43] Errea L F, Mendez L, and Riera A 1982 *J. Phys. B: At. Mol. Phys.* **15** 101
[44] Belyaev A K 2010 *Phys. Rev. A* **82** 060701
[45] Olson R E, Smith F T, and Bauer E 1971 *Appl. Opt.* **10** 1848
[46] Johnson B R 1973 *J. Comput. Phys.* **13** 445
[47] Barnett A R 1982 *Comput. Phys. Commun.* **27** 147
[48] Belyaev A K, Lepetit B, and Gadéa F X 2014 *Phys. Rev. A* **90** 062701